Available online at www.sciencedirect.com
ScienceDirect
Composite Structures 80 (2007) 334–342
COMPOSITE STRUCTURES
www.elsevier.com/locate/compstruct

Online damage detection for laminated composite shells partially filled with fluid

L. Yu [a,b], L. Cheng [a,*], L.H. Yam [a], Y.J. Yan [b], J.S. Jiang [b]

[a] Department of Mechanical Engineering, The Hong Kong Polytechnic University, Hung Hom, Kowloon, Hong Kong, China
[b] Institute of Vibration Engineering, Northwestern Polytechnical University, Xi'an 710072, China

Available online 21 June 2006

Abstract

A general approach for the online damage detection of laminated composite shells partially filled with fluid (LCSFF) is proposed in this paper. Based on advanced composite damage mechanics and the interaction between the fluid and the composite shell, a finite element (FE) model, is first established to simulate the structural response of LCSFF with damage. Piezoelectric patches are used as sensors and actuators to realize automatic damage detections in this FE model. The FE model is validated using structural natural frequencies obtained from experiments. The change in the energy spectrum of the decomposed wavelet signals of structural dynamic responses between the intact and damaged structures is used as the damage index due to its high sensitivity to the structural damage status. The non-linear mapping relationships between the structural damage index and various damage status of the LCSFF are established using an artificial neural network (ANN) trained with numerical structural dynamic response data. Results show that the general approach proposed in this paper can successfully identify the damage status of LCSFF with satisfactory accuracy.

Keywords: Laminated composite shell; Fluid; Damage detection

1. Introduction

Composite shells, either empty or partially filled with fluid, have been extensively used in various sectors of engineering and industry, e.g. aerospace, civil engineering, marine, machine, petrochemical engineering and nuclear power generation. Damage such as cracks or delamination in such shells is inevitable due to a number of factors such as aging, impact, fatigue and chemical corrosion during their service. This usually causes serious fluid leakage problems, leading to catastrophes and economic losses. The automatic detection of such damages in LCSFF is therefore crucial to the safety and cost-effective operation of various composite pipelines and vessels. Therefore, it is necessary to develop a set of feasible and reliable strategy for the online structural damage detection using limited number of sensors. Some of the existing actuating and sensing techniques for obtaining structural damage information and signal analysis are unfortunately too complex to allow an automatic monitoring and detection of structural damages, since in many cases, manual installation and inspection are usually required, and the actuators and sensors are sometimes bulky. For some devices, such as airplanes and spacecraft during flight, chemical engineering facilities located in poisonous or harmful environments and underground pipelines, which are deprived of easy access, it is very difficult to obtain in situ structural damage information. In this regard, the recently developed concept of smart structures offers new possibilities.

Any localized damage in a structure reduces its stiffness, which in turn reduces the natural frequencies and alters the vibration modes of the structure. During the past two decades, extensive researches have been conducted in the area of damage detection based on structural dynamic characteristics using different algorithms and useful databases [1]. Damage modeling in composite structures has been attempted by various researchers in the past. The latest

* Corresponding author. Tel.: +852 2766 6769; fax: +852 2365 4703.
E-mail address: mmlcheng@polyu.edu.hk (L. Cheng).

0263-8223/$ - see front matter © 2006 Elsevier Ltd. All rights reserved.
doi:10.1016/j.compstruct.2006.05.019

effort includes a generalised laminate model featuring both weak interfacial bonding and local delamination by Shu [2]; a plasticity model coupled with the damage and identification for carbon fibre composite laminates by Boutaous et al. [3] and a general FEM model by Yan et al. [4]. As far as the damage index is concerned, a good summary on vibration-based model-dependent damage identification and health monitoring approaches for composite structures can be found in Zou et al. [5]. Araújo dos Santos developed a damage identification technique based on frequency response functions (FRF) sensitivities for laminated structures [6]. Non-linear elastic wave spectroscopy was adopted for the identification of impact damage in a sandwich plate by Meo and Zumpano [7]. Damage detection based on the structural dynamic responses has also been extensively investigated [8,9]. In terms of acquiring and synthesizing information on structural damage status from damage index, owing to their excellent pattern recognition capability, soft computing techniques such as the neural networks [10] and genetic algorithm [11] became very popular in establishing the non-linear mapping relationships between the structural damage index and various damage statuses. Since it is rather difficult to establish an accurate dynamic model for various complex industrial structures, the non-parameter methods based on measured vibration data also arouse extensive interests. In this regard, Staszewski [12] investigated the intelligent signal processing for damage detection in composite materials. Specific techniques such as Lamb wave methods have also been explored [13].

So far, however, most of the vibration-based methods reported in the literature only applied to simple beam-like, plate or truss structures. While a study about the impact response and damage in laminated composite cylindrical shells has been carried out by Krishnamurthy et al. [14], works on online automatic damage detection for LCSFF using methods based on structural dynamics can scarcely be found. In addition, the presence of the fluid and its coupling to the structure in the LCSFF significantly increase the complexity of the problem in terms of both modeling and analysis.

In this paper, an effective damage detection approach for LCSFF is presented. Based on the fluid–structure interaction theory, as well as advanced composite damage mechanics, a dynamic finite element (FE) model of LCSFF is established for carrying out the numerical experiments. The model is then validated using the measured structural natural frequencies. Two embedded piezoelectric patches, one acting as an actuator and the other as a sensor, are simulated in this FE model to obtain structural dynamic responses. The change in energy spectrum of the decomposed wavelet signals of structural dynamic responses [8] is selected as the damage index. Analyses on damage indices of the LCSFF with different fluid surface levels (FSL), ranging from empty to full, show that the selected damage index is effective for composite vessels filled with fluid. Finally, an ANN is trained to further verify the effectiveness of the adopted damage index. It is shown that the ANN can identify the structural damage status of LCSFF with satisfactory accuracy.

2. Finite element model

2.1. Fluid–structural interaction model

The equation of motion for a linear structure can be expressed in the following general form:

$$[M_s]\{\ddot{u}\} + [C_s]\{\dot{u}\} + [K_s]\{u\} = \{F^a\} \tag{1}$$

where $[M_s]$, $[C_s]$ and $[K_s]$ are the structural mass, damping and stiffness matrices, respectively. $\{\ddot{u}\}$, $\{\dot{u}\}$ and $\{u\}$ are the nodal acceleration, velocity and displacement vectors, respectively. $\{F^a\}$ is the applied load vector.

The fluid (water) contained in the LCSFF is assumed to comply with the following assumptions:

1. the fluid is static without sloshing and mean flow;
2. the mean density and pressure are uniform throughout the fluid;
3. the fluid is compressible (density changes due to pressure variations); and
4. the fluid is inviscid with no viscous dissipation.

Then the fluid momentum (Navier–Stokes) and continuity equations can be simplified to get the discretized wave equation as follows:

$$[M_f]\{\ddot{P}_e\} + [C_f]\{\dot{P}_e\} + [K_f]\{P_e\} + \rho_f[R_e]^T\{\ddot{u}\} = 0 \tag{2}$$

where $[M_f]$, $[C_f]$ and $[K_f]$ are the fluid mass, damping and stiffness matrices, respectively. P_e is the nodal pressure vector; ρ_f the mean fluid density; $\rho_f[R_e]$ the coupling mass matrix (at fluid–structure interface) which is given by

$$\rho_f[R_e] = \rho_f \int_s \{N'\}\{N\}^T\{n\}dS \tag{3}$$

where $\{N'\}$ is the element shape function for displacement components u, v, and w (obtained from the structural element); $\{n\}$ the normal at the fluid boundary; $\{N\}$ the element shape function for pressure; S the surface where the derivative of pressure normal to the surface is applied.

In order to fully describe the fluid–structure interaction, the fluid loading acting at the interface should be added to Eq. (1) as:

$$[M_s]\{\ddot{u}\} + [C_s]\{\dot{u}\} + [K_s]\{u\} = \{F^a\} + \{F_e^{pr}\} \tag{4}$$

in which $\{F_e^{pr}\}$ is the fluid loading vector exerted on the interface S, which can be obtained by integrating the pressure over the area of the surface:

$$\{F_e^{pr}\} = \int_S \{N'\}\{n\}P\,dS \tag{5}$$

The finite element approximate function P for fluid pressure is given by

$$P = \{N\}^T\{P_e\} \tag{6}$$

Combining Eqs. (5) and (6) yields

$$\{F_e^{pr}\} = \int_S \{N'\}\{N\}^T\{n\}dS\{P_e\} \tag{7}$$

By comparing the integral in Eq. (7) with the definition of coupling mass matrix (at fluid–structure interface) $\rho_f[R_e]$ in Eq. (3), it becomes clear that:

$$\{F_e^{pr}\} = [R_e]\{P_e\} \tag{8}$$

Then, substitution of Eq. (8) into Eq. (4) results in the structural elemental equation of motion:

$$[M_s]\{\ddot{u}\} + [C_s]\{\dot{u}\} + [K_s]\{u\} - [R_e]\{P_e\} = \{F^a\} \tag{9}$$

Eqs. (2) and (9) provide a complete set of discretized finite element equations for the fluid–structure interaction problem and can be written in an assembled form as:

$$\begin{bmatrix} [M_s] & [0] \\ [M^{fs}] & [M_f] \end{bmatrix} \begin{Bmatrix} \{\ddot{u}\} \\ \{\ddot{P}_e\} \end{Bmatrix} + \begin{bmatrix} [C_s] & [0] \\ [0] & [C_f] \end{bmatrix} \begin{Bmatrix} \{\dot{u}\} \\ \{\dot{P}_e\} \end{Bmatrix} + \begin{bmatrix} [K_s] & [K^{fs}] \\ [0] & [K_f] \end{bmatrix} \begin{Bmatrix} \{u\} \\ \{P_e\} \end{Bmatrix} = \begin{Bmatrix} \{F^a\} \\ \{0\} \end{Bmatrix} \tag{10}$$

where $[M^{fs}] = \rho_f[R_e]^T$ and $[K^{fs}] = -[R_e]$.

2.2. Verification of the FE model

The validity of this FE model is verified using measured natural frequencies. The verification consists of two parts.

(1) Using the present FE model, a typical clamped-free thin wall steel cylindrical storage tank partially filled with water is simulated. Results are compared with the numerical and experimental results reported in Ref. [15]. The steel cylindrical shell has a mean radius $R = 36$ mm, wall thickness $t = 1.5$ mm and length $L = 231$ mm. Its material properties are: Young's modulus $E = 205$ GPa, Poisson's ratio $v = 0.3$ and density $\rho = 7800$ kg/m^3. The shell is filled with water up to a level H (see Fig. 1). The lowest 10 natural frequencies for $H/L = 0.697$ are considered. Results acquired by experiment, numerical simulation in Ref. [15] and the present numerical simulation are listed in Table 1 as f_1, f_2 and f_3, respectively. Errors of the two numerical simulation results with respect to experimental results are also calculated, and listed as ε_{21} and ε_{31} in Table 1, respectively. Since the natural frequencies of some lower order modes of the shell structure are highly sensitive to the boundary conditions set in the FEM model, which is very difficult to achieve in experiments, errors between the experimentally measured and numerically simulated data are relatively large for some modes. Nevertheless, the present model agrees reasonably well with the experimental data. In general its accuracy seems to exceed that of Ref. [15]. It can be concluded that the FEM program used in this study is accurate enough in dealing with fluid–structure interaction problem.

(2) The experimental measurements of natural frequencies of an empty laminated composite shell and LCSFF were carried out. The dimensions of the LCSFF specimen

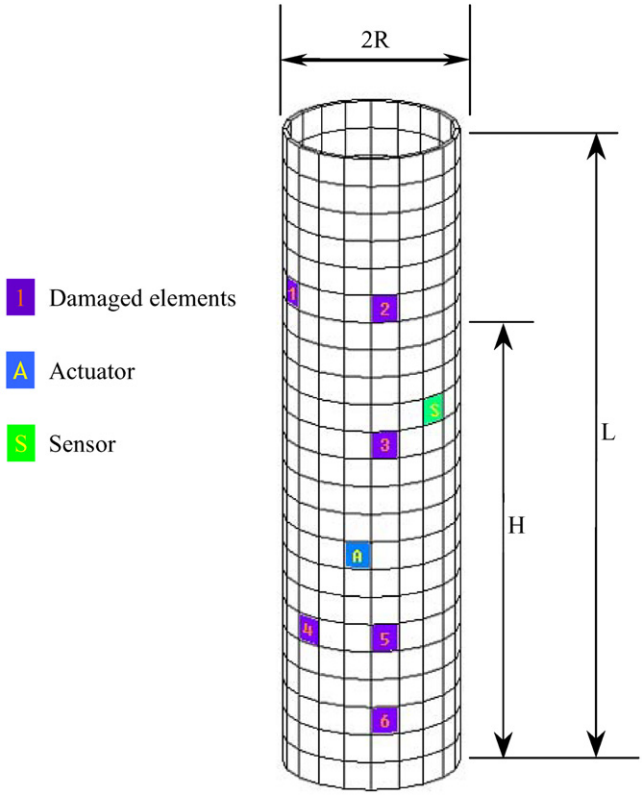

Fig. 1. Model of a composite shell partially filled with fluid.

are: mean radius $R = 36$ mm, wall thickness $t = 2$ mm, and length $L = 280$ mm (also shown in Fig. 1). The shell is made of resin glass fibre with orthogonal layer $(-45°/45°)_{30}$, which has the following material characteristics: $E_1 = 47.518$ GPa, $E_2 = 4.588$ GPa, $G_{12} = 2.10$ GPa, $\mu_{12} = 0.4495$, $\mu_{21} = 0.0434$, and $\rho = 1860$ kg/m^3. The FE model of the wall of this LCSFF consists of 460 (23×20) eight-node shell elements with three degrees of freedom (DOF) at each node [16,17]. The FE model of the bottom of this LCSFF consists of 62 shell elements of the same type. For the LCSFF partially filled with water ($H/L = 0.5678$) 806 3-D fluid elements [18] are used. The dimension and meshing of the LCSFF model are shown in Fig. 1.

During experiment, the LCSFF specimen was put on a large piece of soft sponge to achieve free boundary conditions. The frequency response function was measured using a Brüel & Kjær (B&K) 2035 Signal Analyzer Unit. The structure was excited by a B&K 8206 impact hammer and the responses were measured by B&K 4397 piezoelectric deltaShear accelerometers connected to a B&K Charge Amplifier Type 2635 (see Fig. 2).

The measured magnitudes of the frequency response function for empty shell and shell partially filled with water ($H/L = 0.5678$) are shown in Fig. 3. It can be seen that the dynamic property of the shell changes with the contained water. It is obvious that the resonant frequencies decrease as the water level H/L increases due to the mass loading effect of the fluid. The measured and computed natural frequencies for $H/L = 0$ and 0.5678 are tabulated in Tables 2

Table 1
Natural frequencies of the cylindrical shell filled with water, $H/L = 0.697$

Experimental results [15], f_1 (Hz)	FEM results [15], f_2 (Hz)	ε_{21} (%) $\left(\left\|\frac{f_2-f_1}{f_1}\right\|\%\right)$	FEM results using present model, f_3 (Hz)	ε_{31} (%) $\left(\left\|\frac{f_3-f_1}{f_1}\right\|\%\right)$
522	543.1	4.042	525.43	0.657
582	672.7	15.584	625.29	7.438
798	806	1.003	802.45	0.558
1196	1188.4	0.635	1227.3	2.617
1244	1253.2	0.740	1236.6	0.595
–	1407.4	–	1297.7	–
1394	1425.3	2.245	1456	4.447
1546	1553.8	0.505	1538.7	0.472
–	1679.7	–	1592	–

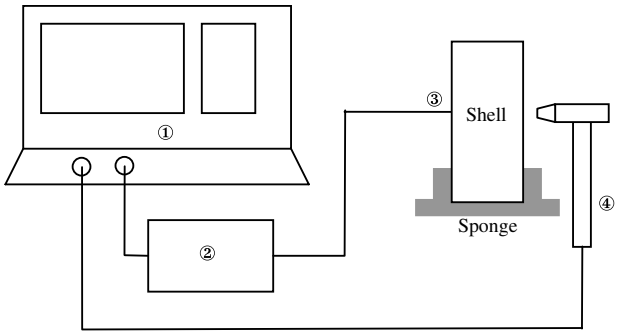

① Brüel & Kjær (B&K) 2035 Signal Analyzer Unit
② B&K Charge Amplifier Type 2635
③ B&K 4397 piezoelectric deltaShear accelerometers
④ B&K 8206 impact hammer

Fig. 2. Schematic diagram of the experimental set-up for LCSFF.

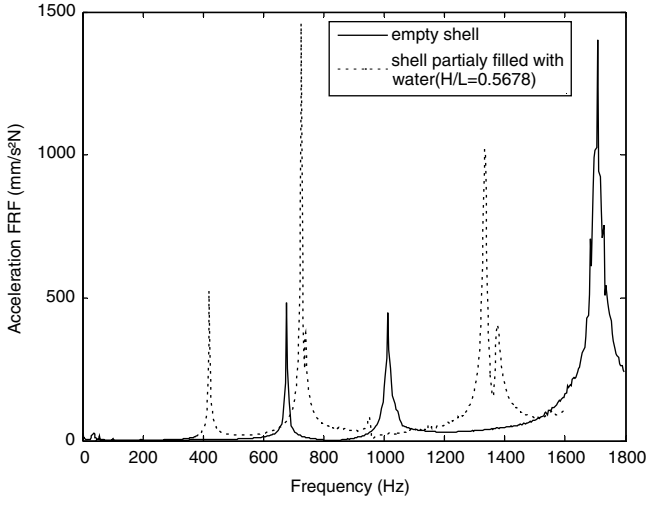

Fig. 3. The measured frequency response function of the LCSFF with $H/L = 0$ and 0.5678.

and 3, respectively. Since the LCSFF under investigation is axially symmetrical, all natural frequencies listed in Tables 2 and 3 are repeated natural frequencies, so only the odd number order ones are listed. Table 2 shows a maximum error of 4.66% for the first six natural frequencies for the empty composite shell. Table 3 shows that the average

Table 2
Natural frequencies of the laminated composite cylindrical shell with $H/L = 0$

Experiment results (Hz)	FEM results (Hz)	Error (%)
638	640.48	0.3716
1006	1019.2	1.2951
1712	1795.6	4.66

Table 3
Natural frequencies of the laminated composite cylindrical shell filled with water with $H/L = 0.5678$

Experiment results (Hz)	FEM results (Hz)	Error (%)
422	424.84	0.668487
728	734.92	0.941599
954	984.72	3.119669
1336	1355.2	1.416765
1380	1401.6	1.541096

error is 1.537% and the maximum error is 3.12% for the first 10 natural frequencies of the LCSFF with water level $H/L = 0.5678$. Therefore, the agreement between numerical and experimental results is generally satisfactory. The proposed FE model can provide enough accuracy in dealing with fluid contained structures made of composite materials.

2.3. Mathematical formulation of piezoelectric sensors and actuators

Embedded and/or surface mounted piezoelectric patches are widely used in online damage detection due to their advantage in sensitivity, weight and volume. Based on previous numerical [8] and experimental work [19,20], simulation on piezoelectric sensors and actuators in FE model is feasible in numerical study of damage detection.

When piezoelectric patches are embedded into the composite shell as sensors and actuators, the direct and converse piezoelectric equations with respect to the reference coordinate axes can be written as follows [21]

$$\{\sigma_P\} = [Q_P]\{\varepsilon\} - [e]^T\{E\} \quad (11)$$

$$\{D\} = [e]\{\varepsilon\} + [\bar{\varepsilon}]\{E\} \quad (12)$$

where $\{\sigma_P\}$ and $[Q_P]$ are the stress vector and the transformed elastic stiffness matrix of the piezoelectric material, respectively; $\{\varepsilon\}$ the strain vector; $\{E\}$ the electric field vector; $\{D\}$ the electric displacement vector; $[\bar{\varepsilon}]$ the permittivity matrix and $[e]^T$ the transpose of $[e]$. The piezoelectric stress coefficient matrix $[e]$ is expressed in terms of the strain coefficient matrix $[d]$ as

$$[e] = [d][Q_P] \tag{13}$$

A thin piezoelectric patch, polarized only in the thickness direction, exhibits transversely isotropic properties in the plane perpendicular to the thickness direction. Eqs. (11) and (12) can then be written as

$$\begin{Bmatrix} \sigma_x \\ \sigma_y \\ \tau_{yz} \\ \tau_{zx} \\ \tau_{xy} \end{Bmatrix} = \begin{bmatrix} Q_{P11} & Q_{P12} & 0 & 0 & 0 \\ Q_{P21} & Q_{P22} & 0 & 0 & 0 \\ 0 & 0 & Q_{P44} & 0 & 0 \\ 0 & 0 & 0 & Q_{P55} & 0 \\ 0 & 0 & 0 & 0 & Q_{P66} \end{bmatrix} \begin{Bmatrix} \varepsilon_x \\ \varepsilon_y \\ \gamma_{yz} \\ \gamma_{zx} \\ \gamma_{xy} \end{Bmatrix} + [Q_P]^T \begin{bmatrix} 0 & 0 & d_{31} \\ 0 & 0 & d_{31} \\ 0 & d_{15} & 0 \\ d_{15} & 0 & 0 \\ 0 & 0 & 0 \end{bmatrix} \begin{Bmatrix} 0 \\ 0 \\ E_3 \end{Bmatrix} \tag{14}$$

$$\begin{Bmatrix} D_1 \\ D_2 \\ D_3 \end{Bmatrix} = \begin{bmatrix} 0 & 0 & 0 & d_{15} & 0 \\ 0 & 0 & d_{15} & 0 & 0 \\ d_{31} & d_{31} & 0 & 0 & 0 \end{bmatrix} [Q_P] \begin{Bmatrix} \varepsilon_x \\ \varepsilon_y \\ \gamma_{yz} \\ \gamma_{zx} \\ \gamma_{xy} \end{Bmatrix} + \begin{bmatrix} \bar{\varepsilon}_{11} & 0 & 0 \\ 0 & \bar{\varepsilon}_{22} & 0 \\ 0 & 0 & \bar{\varepsilon}_{33} \end{bmatrix} \begin{Bmatrix} 0 \\ 0 \\ E_3 \end{Bmatrix} \tag{15}$$

where E_3 is the electric field intensity exerted on piezoelectric materials in the thickness direction, and can be expressed as

$$E_3 = \frac{V_3(t)}{t_p} \tag{16}$$

where $V_3(t)$ is the applied voltage and t_p is the thickness of the piezoelectric actuator.

3. Detection of structural crack damage

3.1. Crack damage and its effect on the stiffness of a composite structure

In the FE model, the crack damage is simulated by modifying the elastic moduli of the damaged element. For composite materials with crack damages, variations of local elastic modulus can be calculated as follows [22]

$$\left.\begin{aligned} E_1 &= E_1^0 + 2\omega_3(C_3 + C_6(\mu_{12}^0)^2 - C_{12}\mu_{12}^0) \\ E_2 &= E_2^0 + 2\omega_3(C_6 + C_3(\mu_{21}^0)^2 - C_{12}\mu_{21}^0) \\ \mu_{12} &= \mu_{12}^0 + \omega_3 \tfrac{1-\mu_{12}^0\mu_{21}^0}{E_2^0}(C_{12} - 2C_6\mu_{12}^0) \\ \mu_{21} &= \tfrac{E_2}{E_1}\mu_{12}, \quad \mu_{12} \gg \mu_{21} \\ G_{12} &= \tfrac{E_2}{2(1+\mu_{12})}, \quad G_{23} = G_{13} = G_{12} \end{aligned}\right\} \tag{17}$$

where E_1, E_2, μ_{12}, μ_{21} and G_{12} are the elastic moduli, Poisson's ratios and shear modulus of the thin wall composite shell with crack damage, respectively. E_1^0, E_2^0, μ_{12}^0, μ_{12}^0 and G_{12}^0 are the elastic moduli, Poisson's ratios and shear modulus of the intact composite structure, respectively. C_1–C_{12} are material coefficients independent of strains and damage, but dependent on the composite configuration, i.e., fibre geometry and orientations, fibre volume fraction, ply stacking sequence, etc. These parameters can be determined by measuring the specimen made of the same composite materials [22]. Let ω_3 be a variable representing the crack damage status, which is related to the number, length and width of the crack. It can be expressed as

$$\omega_3 = \eta_c \bar{a}_c \bar{b}_c \bar{f}_c \tag{18}$$

where η_c is the crack density, which is defined as the crack number in a unit area; $\bar{a}_c$ and $\bar{b}_c$ are the average length and width of the crack, respectively, and $\bar{f}_c$ is an adjustment coefficient, which has been discussed in Ref. [22].

For other types of damage in a resin glass fibre structure, such as delamination, the variations of local elastic modulus can also be calculated using Eq. (17) with its corresponding material coefficients.

3.2. Index of damage

Generally speaking, changes in structural dynamic properties due to structural damage are very small. Yan and Yam [8] pointed out that when the crack length in a composite plate reached 1% of the plate length, the relative variation of the structural natural frequencies was generally about 0.01–0.1%. Therefore, using vibration modal parameters, e.g., natural frequencies, displacement or strain mode shapes, and modal damping factors is generally ineffective in identifying small and incipient structural damage. The revelation of small and incipient damage in in-service structures has important applied values, because it can monitor the occurrence and development of structural damage. Therefore, a sensitive indicator needs to be found to show the change of the response data caused by damage. Chui [23] pointed out that the local singularity in a time-sequence signal could be more clearly exhibited if the signal is decomposed using wavelet transform. This idea has been successfully applied to vibration-based structural damage detection in many works [8,20,24–26]. When structural vibration response signals in time domain are decomposed into multiple sub-signals using wavelet transform, the

change in each sub-signal corresponding to structural damage may manifest notable difference. The percentage change of energy spectra between the intact and damaged structures is therefore taken as the feature index of structural damage. It has been observed that the energy spectrum of the decomposed wavelet signal obtained from structural vibration responses can indicate the structural damage status with higher sensitivity. Even the ratio of the damage size to the total structural size retreats to the order of 0.01–0.1%, the structural damage can still be detected using energy spectrum variation obtained by wavelet analysis [8]. So in the present study, the variation of the energy spectrum of decomposed wavelet signal is used as the index of damage.

The wavelet transform of a continuous vibration response $x(t)$ is defined as

$$W_x(a,b) = (|a|)^{-\frac{1}{2}} \int_R x(t) \Psi^* \left(\frac{t-b}{a} \right) \mathrm{d}t \tag{19}$$

where b is the translation parameter; a the scale parameter; $x(t)$ the vibration response to be decomposed; $\Psi^*(t)$ the transforming function (mother wavelet); and W_x the calculated wavelet coefficients, which can be used to recompose the original function $x(t)$. The recomposed equation for $x(t)$ can be expressed as

$$x(t) = \frac{1}{C_\Psi} \int_{-\infty}^{+\infty} \int_{-\infty}^{+\infty} \frac{1}{a^2} W_x(a,b) \Psi \left(\frac{t-b}{a} \right) \mathrm{d}a \, \mathrm{d}b \tag{20}$$

where $C_\Psi = 2\pi \int_0^{+\infty} (|\Psi(r)|)^2 \mathrm{d}r/r$.

Various forms of wavelet base function $\Psi(t)$ have been developed. One of the most useful practical methods for signal decomposition is the wavelet packet analysis (WPA) [27]. The WPA algorithm is as follows:

Let $g_j^n(t) \in U_j^n$, then $g_j^n(t)$ can be expressed as

$$g_j^n(t) = \sum_l d_l^{j,n} u_n(2^j t - l) \tag{21}$$

In WPA decomposition algorithm, $\{d_l^{j,2n}\}$ and $\{d_l^{j,2n+1}\}$ can be calculated as follows:

$$\left. \begin{aligned} d_l^{j,2n} &= \sum_k a_{k-2l} d_k^{j+1,n} \\ d_l^{j,2n+1} &= \sum_k b_{k-2l} d_k^{j+1,n} \end{aligned} \right\} \tag{22}$$

and the formula for recomposing $\{d_l^{j+1,n}\}$ using $\{d_l^{j,2n}\}$ and $\{d_l^{j,2n+1}\}$ is

$$d_l^{j+1,n} = \sum_k \left[h_{l-2k} d_k^{j,2n} + g_{l-2k} d_k^{j,2n+1} \right] \tag{23}$$

The WPA method can adaptively choose the corresponding frequency bandwidth according to the characteristics of the signal to be analyzed, and the decomposed sub-wavelet functions possess orthogonality in both frequency and time domains.

Assuming that the original vibration response $x_{0,0}^{(i)}(t)$ at the ith measurement location of a structure is decomposed into $x_{L,j}^{(i)}(t)$ $(j = 1, 2, \ldots, 2^{L-1})$, with L being the selected layer number of the wavelet tree, $x_{0,0}^{(i)}(t)$ can then be expressed as

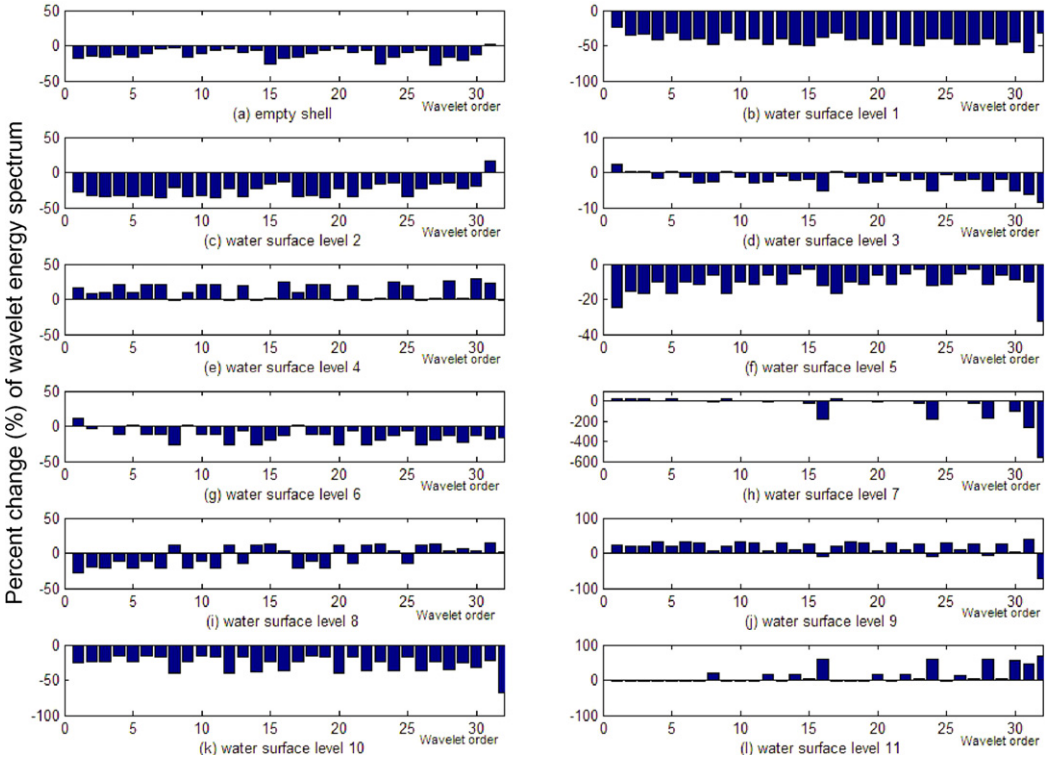

Fig. 4. Damage indices for the same damage with different water surface levels.

$$x_{0,0}^{(i)}(t) = \sum_{j=1}^{2^{L-1}} x_{L,j}^{(i)}(t) \tag{24}$$

Let the energy of the jth order sub-signals of the intact and damaged structures be $U_{L,j}^0$ and $U_{L,j}^d$, respectively. A non-dimensional damage feature index vector can be composed as follows:

$$V_{\mathrm{d}} = \{v_1, v_2, \ldots, v_{2^{L-1}}\}^{\mathrm{T}} = \left\{1 - \frac{U_{L,1}^d}{U_{L,1}^0}, 1 - \frac{U_{L,2}^d}{U_{L,2}^0}, \ldots, 1 - \frac{U_{L,2^{L-1}}^d}{U_{L,2^{L-1}}^0}\right\}^{\mathrm{T}} \tag{25}$$

Generally, different structural damage types, locations and severities will match one by one with different damage feature index vectors. Therefore, the element values of different damage feature index vector V_{d} can not only show the differences between the intact and damaged structures, but also indicate the changes of different structural damage status.

4. Damage index and damage identification of LCSFF by ANN

4.1. Damage index for LCSFF

In this study the damage indices are expressed in terms of the percentage changes in the energy spectrum of the decomposed wavelet signals of structural dynamic response due to damage. There is a crack in the LCSFF model with a length $\bar{a}_{\mathrm{c}} = 3$ mm and a width $\bar{b}_{\mathrm{c}} = 0.1$ mm at location 6 as shown in Fig. 1. For this damaged shell the damage indices measured for twelve gradually increasing water surface levels in the shell from $H/L = 0$ (empty shell) to $H/L = 1$ (fully-filled) are shown in Fig. 4. It can be seen that most of the water-contained shells have larger damage index values than the empty shell. Therefore, compared with the empty shell, the presence of fluid in the structure does not reduce the sensitivity of the damage index.

It should also be noted that the locations of the sensors and actuators are important for damage detection. For shell with water lever 3, the absolute value of the damage index is relatively small and is less than 10%, while it reaches more than 500% for water lever 7. This suggests that an optimization on the locations of sensors and actuators is worthy of further study.

4.2. Identification of structural damage status by ANN

As an example, one ANN for LCSFF with $H/L = 0.5678$ is designed and trained. The vibration responses of 321 different cases are numerically simulated using FEM, and in all these cases, $H/L = 0.5678$. These 321 cases include an intact LCSFF, LCSFFs with crack damage at 80 different locations of the shell, each with four different crack lengths (1–8% of the LCSFF height). Then, damage indices of these 320 damage cases are obtained by comparing the energy spectrum of the decomposed wavelet signals for each case with that of the intact structure. From these damage cases, six cases are selected as verification samples, with their locations shown in Fig. 1. The other 314 damage cases are used as train samples. The mesh in present FE model is regular. Then the elements in the shell can be located by its row and column number. The row number is counted from top to bottom of the model. The column number is counted clockwise and the column containing the sensor is selected as the first column. The row and column number are unified by dividing them by 23 (the total row number) and 20 (the total column number), respectively. The lengths of the cracks are expressed in permillage of the LCSFF height. One back propagation (BP) neural network, possessing 32 inputs, one hidden layer with 16 nodes and three outputs, is designed (Fig. 5). The inputs are 32 elements of the damage index, and the outputs are the row and column number of the damaged element, and the length of the crack. After trained with 314 samples for 1142 epochs, the performance goal is achieved (Fig. 6).

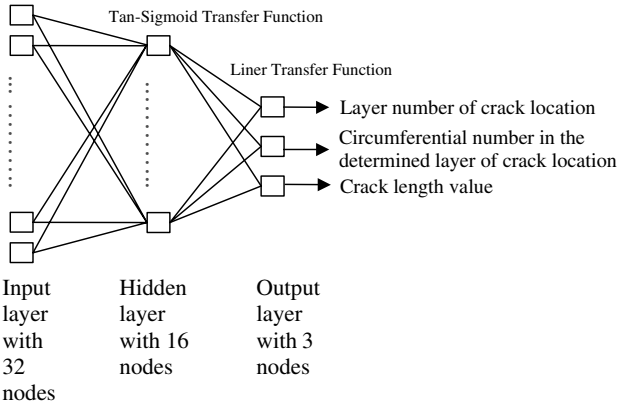

Fig. 5. Structure of a BP neural network for identification of crack length and location.

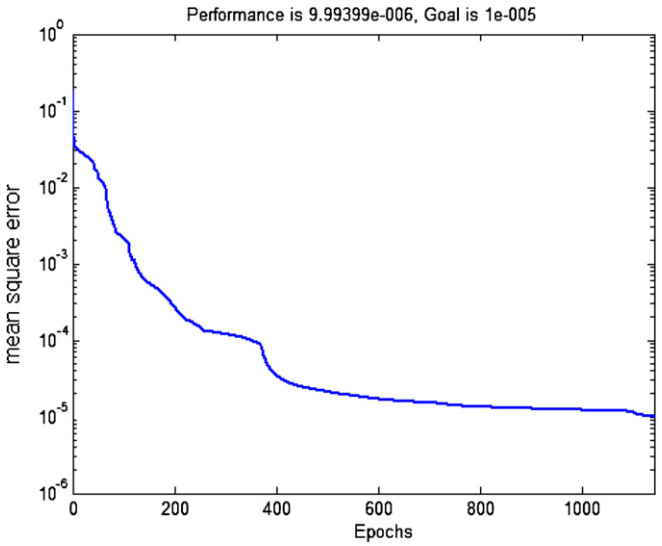

Fig. 6. The error of BP neural network in the training process.

Table 4
Identification of crack damage using the trained ANN (crack location and length)

	Case 1	Case 2	Case 3	Case 4	Case 5	Case 6
Row number of damage element (real)	6.000	6.000	11.000	18.000	18.000	21.000
Row number of damage element detected by ANN	6.088	6.054	11.222	18.382	18.215	21.171
Column number of damage element (real)	6	2	2	5	2	2
Column number of damage element detected by ANN	5.879	2.037	1.991	4.923	2.026	1.971
Crack length value (real) (%)	2.000	7.000	8.000	3.000	6.000	8.000
Crack length value detected by ANN (%)	2.014	7.031	8.152	3.044	5.988	8.119

Results for six sets of verification samples obtained by numerical simulation using FEM are listed in Table 4. (The row and column numbers listed in Table 4 are converted to their actual values by multiplying them by the total numbers of row and column, respectively. The lengths of cracks listed in Table 4 are converted to percentage of the LCSFF height.) It shows that the identified crack status is very close to the actual crack status.

5. Conclusions

In this paper a dynamic FE model of LCSFF is established by considering the interaction between fluid and the composite shell. Two piezoelectric patches embedded into the composite shell, one serving as an actuator and the other as a sensor, are included in the FE model for obtaining the numerically simulated structural dynamic responses. The advanced composite damage mechanics is used to simulate the crack, and the change in energy spectrum of the decomposed wavelet signals of structural dynamic responses is used as the damage index due to its high sensitivity to structural damage. The reliability of the model is verified using the experimentally measured structural natural frequencies. Effects of fluid contained in the composite vessel on structural damage index are investigated. Damage detection using a BP neural network for a LCSFF with $H/L = 0.5678$ is successfully carried out. It shows that the general approach proposed in this paper, including the use of smart elements, damage index and the ANN, provides an effective tool for LCSFF damage detection applications.

Acknowledgements

The authors would like to thank for the support by the Research Grants Council of Hong Kong Special Administrative Region of China under the Project No. PolyU 5313/03E; and Natural Science Foundation of China under the grant 50375123. The second author wishes to acknowledge the support from a special fund for recently promoted Chair Professors given by The Hong Kong Polytechnic University.

References

[1] Carden PE, Fanning P. Vibration based condition monitoring: a review. Struct Health Monit 2004;3(4):355–77.
[2] Shu XP. A generalised model of laminated composite plates with interfacial damage. Compos Struct 2006;74:237–46.
[3] Boutaous A, Peseux B, Gornet L, et al. A new modeling of plasticity coupled with the damage and identification for carbon fibre composite laminates. Compos Struct 2006;74:1–9.
[4] Yan YJ, Yam LH, Cheng L, Yu L. FEM modeling method of damage structures for structural damage detection. Comput Struct 2006;72:193–9.
[5] Zou Y, Tong L, Steven GP. Vibration-based model-dependent damage (delamination) identification and health monitoring for composite structures – a review. J Sound Vib 2000;230:357–78.
[6] Araújo dos Santos JV, Mota Soares CM, Mota Soares CA, Maia NMM. Structural damage identification in laminated structures using FRF data. Compos Struct 2005;67:239–49.
[7] Meo M, Zumpano G. Nonlinear elastic wave spectroscopy identification of impact damage on a sandwich plate. Compos Struct 2005;71:469–74.
[8] Yan YJ, Yam LH. Online detection of crack damage in composite plates using embedded piezoelectric actuators/sensors and wavelet analysis. Compos Struct 2002;58:29–38.
[9] Chen Q, Chan YW, Worden K. Structural fault diagnosis and isolation using neural networks based on response-only data. Comput Struct 2003;81:2165–72.
[10] Pierce SG, Worden K, Manson G. A novel information-gap technique to assess reliability of neural network-based damage detection. J Sound Vib 2006;293:96–111.
[11] Kang YL, Lin XH, Qin QH. Inverse/genetic method and its application in identification of mechanical parameters of interface in composite. Comput Struct 2004;66:449–58.
[12] Staszewski WJ. Intelligent signal processing for damage detection in composite materials. Compos Sci Technol 2002;62:941–50.
[13] Su ZQ, Ye L. Lamb wave-based quantitative identification of delamination in CF/EP composite structures using artificial neural algorithm. Compos Struct 2004;66:627–37.
[14] Krishnamurthy KS, Mahajan P, Mittal RK. Impact response and damage in laminated composite cylindrical shells. Compos Struct 2003;59:15–36.
[15] Mazúch T, Horacek J, Trnka J, Veselý J. Natural modes and frequencies of a thin clamped-free steel cylindrical storage tank partially filled with water: FEM and measurement. J Sound Vib 1996;193:669–90.
[16] Fenves SJ. Numerical and computer methods in structural mechanics. New York: Academic Press, Inc.; 1973.
[17] Taylor RL, Beresford PJ, Wilson EL. A non-conforming element for stress analysis. Int J Numer Methods Eng 1976;10:1211–9.
[18] Mazúch T. Determining the acoustic natural modes and frequencies of irregular shaped rigid walled cavities by FEM. J Czech Slovak Mech Eng 1993;44:433–40.
[19] Banks HT, Inman DJ, Leo DJ, Wang Y. An experimentally validated damage detection theory in smart structures. J Sound Vib 1996;191:859–80.
[20] Yam LH, Yan YJ, Jiang JS. Vibration-based damage detection for composite structures using wavelet transform and neural network identification. Compos Struct 2003;60:403–12.
[21] Rosen CZ. Piezoelectricity. New York: American Institute of Physics; 1992.

[22] Talreja R. Damage mechanics of composite materials. Composite materials series, vol. 9. Amsterdam: Elsevier; 1994.
[23] Chui CK. Wavelets: a mathematical tool for signal processing. Philadelphia, PA: Society for Industrial and Applied Mathematics; 1997.
[24] Liew KM, Wang Q. Application of wavelet theory for crack identification in structures. J Eng Mech 1998;124(2):152–7.
[25] Hou Z, Noori M, Amand RSt. Wavelet-based approach for structural damage detection. J Eng Mech ASCE 2000;126:677–83.
[26] Lu C, Hsu Y. Vibration analysis of an inhomogeneous string for damage detection by wavelet transform. Int J Mech Sci 2002;44:745–754.
[27] Jones CL, Lonergan GT, Mainwaring DE. Wavelet packet computation of the Hurst exponent. J Phys A: Math Gen 1996;29:2509–27.